

Quantum Wigner solid in two-dimensional electron systems in semiconductors

Alexander A. Shashkin^a and Sergey V. Kravchenko^b

^aInstitute of Solid State Physics, Chernogolovka, Moscow District 142432, Russia

^bPhysics Department, Northeastern University, Boston, MA 02115, USA

ARTICLE HISTORY

Compiled December 1, 2025

ABSTRACT

We review recent transport experiments that reveal two-threshold voltage-current characteristics, marked by a significant increase in noise between the two threshold voltages, at low electron densities in the insulating regime in two-dimensional (2D) electron systems, specifically in silicon metal-oxide-semiconductor field-effect transistors (MOSFETs) and SiGe/Si/SiGe heterostructures. The double-threshold voltage-current characteristics closely resemble those observed in the collective depinning of the vortex lattice in type-II superconductors. By adapting the model used for vortices to the case of an electron solid, good agreement with the experimental results is achieved, which supports a quantum electron solid forming in the low electron density state. When a perpendicular magnetic field is applied, the double-threshold behavior occurs at voltages an order of magnitude lower and at significantly higher electron densities than the zero-field case. This indicates the stabilization of the quantum electron solid, aligning with theoretical predictions. Interestingly, the double-threshold voltage-current curves, indicative of electron solid formation at low densities, are not observed in the quantum Hall regime. This lack of observation does not confirm the existence of a quasi-particle quantum Hall Wigner solid and indicates that quasi-particles near integer filling do not form an independent subsystem.

KEYWORDS

Condensed matter physics, Strongly correlated electrons, Two-dimensional electron systems, Wigner crystal

Contents

1	Introduction	2
2	Materials and Methods	3
3	Results and Discussions	4
3.1	Double-threshold voltage-current curves as a signature of quantum electron solid; results obtained in Si MOSFETs	4
3.2	Generality of the double-threshold voltage-current curves for different classes of electron systems; results obtained in SiGe/Si/SiGe heterostructures	8
3.3	Stabilization of the quantum electron solid in perpendicular magnetic fields in SiGe/Si/SiGe heterostructures	13
3.4	Inequivalence of the low-density insulating state and quantum Hall insulating states in SiGe/Si/SiGe heterostructures	17
4	Conclusions	19

1. Introduction

Experimental investigations into the transport and thermodynamic properties of two-dimensional (2D) electrons in semiconductors have indicated that these systems may approach a phase transition to an unknown state at low electron densities. This new state could be a quantum Wigner crystal or a precursor [1–11]. The term quantum refers to the fact that, in this context, the Fermi energy governs the kinetic energy of 2D electrons, in contrast to the classical Wigner crystal [12], where the kinetic energy is determined by temperature. The phase transition point in the least-disordered 2D electron systems in semiconductors is near the critical electron density for the metal-insulator transition, below which the 2D electrons become localized. Although the insulating regime of the metal-insulator transition has been extensively studied [13–27], there has been no definitive conclusion regarding the origin of the low-density state. Single-threshold current-voltage ($I - V$) curves have been observed, which can be interpreted either as a sign of the depinning of an electron solid [14,15,18,19] or as a breakdown of the insulating phase, consistent with traditional scenarios like strong electric field Efros-Shklovskii variable range hopping [28] or percolation (see, *e.g.*, Refs. [17,29–31] and the references therein). Attempts to observe broadband voltage noise at the threshold of these $I - V$ curves and to probe the low-density state in perpendicular magnetic fields have not yielded sufficient information to clearly differentiate between the depinning of the electron solid and traditional mechanisms [17,30,31]. It is important to note that much confusion has arisen because many authors have chosen to interpret their data in the context of the Wigner crystal, overlooking conventional interpretations.

An important advance in uncovering the origin of the low-density state in strongly correlated 2D electron systems has been reported in Ref. [32]. Two-threshold $V - I$ characteristics have been observed, marked by a dramatic increase in noise between the two threshold voltages at the breakdown of the low-electron-density insulating phase. This noise manifests itself as strong current fluctuations; it rises significantly above the first threshold voltage V_{th1} and essentially disappears above the second

threshold voltage $V_{\text{th}2}$. The sharp noise peak in the $V - I$ curves illustrates the double-threshold behavior. This phenomenon resembles the collective depinning of the vortex lattice in Type-II superconductors, with the voltage and current axes interchanged. The findings strongly favor the sliding 2D quantum electron solid, whereas the double-threshold behavior cannot be described within alternative scenarios such as percolation or overheating. It should be emphasized that, rather than being an ideal Wigner crystal, the 2D electron system studied is likely to be closer to an amorphous solid, similar to the vortex lattice in Type-II superconductors, where collective pinning has been well established. In previous studies, where the current was passed through the sample and the voltage between potential probes was measured, no distinct features were observed on almost flat curves in the breakdown regime. The main problem with those studies was that the noise in the voltage signal was small, which prevented the identification of a second threshold voltage. In contrast, a DC voltage was applied between the source and the drain and the resulting induced current was measured. It was found that in this measurement configuration, the current noise is clear and dramatic. As a result, this experimental approach allowed the discovery of features that had not been previously observed.

Below, we describe transport experiments on Si MOSFETs and ultra-high-mobility SiGe/Si/SiGe heterostructures in both zero and perpendicular magnetic fields.

2. Materials and Methods

Two sets of samples were utilized: silicon MOSFETs and SiGe/Si/SiGe heterostructures. Measurements were performed in an Oxford dilution refrigerator with a base temperature of approximately 30 mK. The direct current (DC) and noise were recorded using an ultra-low-noise current-voltage converter connected to a digital voltmeter or a lock-in amplifier.

The silicon (100) MOSFETs exhibited a peak electron mobility of approximately $3 \text{ m}^2 \text{ V}^{-1} \text{ s}^{-1}$ at temperatures below 0.1 K, which is similar to the values reported in Ref. [33]. The electron density was controlled by applying a positive DC voltage to the gate in relation to the contacts, with an oxide thickness of 150 nm. The samples were designed with a Hall bar geometry, measuring $50 \mu\text{m}$ in width.

Thin gaps were added to the gate metallization to tackle the primary experimental challenge of high contact resistance in the low-density, low-temperature regime. This design facilitated the maintenance of a high electron density near the contacts, independent of the density in the main section of the sample. As a result, contact resistances did not exceed approximately $10 \text{ k}\Omega$, allowing them to be disregarded in the insulating state. The voltage-current ($V - I$) characteristics and noise were measured in the central part of the sample, which had a length of $180 \mu\text{m}$.

To create a SiGe/Si/SiGe sample, ultra-clean UHCVD-grown SiGe/Si/SiGe quantum wells (for details, see Refs. [34–36]) were utilized. The electron mobility in these samples at low temperatures reached approximately $200 \text{ m}^2/\text{Vs}$, which is higher than that observed in previously used SiGe-based structures [34–37]. A silicon (001) quantum well, approximately 15 nm wide, was sandwiched between $\text{Si}_{0.8}\text{Ge}_{0.2}$ potential barriers [38]. Contacts to the 2D layer were established using an approximately 300 nm thick $\text{Au}_{0.99}\text{Sb}_{0.01}$ alloy, which was deposited using a thermal evaporator and then annealed for 3-5 minutes at 440°C in an N_2 atmosphere. Through photolithography, the samples were patterned into Hall-bar shapes with a $150 \mu\text{m}$ distance between the potential probes and a width of $50 \mu\text{m}$. An approximately 80 nm thick SiO layer was

deposited on the wafer surface using a thermal evaporator, followed by depositing an approximately 40 nm thick aluminum gate on top of the SiO layer. Additionally, a roughly 20 nm thick layer of NiCr was applied on top of the aluminum to improve the adhesion of subsequent layers. The contact gate was then fabricated, for which the structure was covered with an approximately 200 nm thick SiO layer, followed by an approximately 60 nm thick aluminum gate deposited on top of the SiO. The contact gate was designed to maintain a high electron density of about $2 \times 10^{11} \text{ cm}^{-2}$ near the contact areas, independent of the electron density in the main part of the sample. No intentional doping was applied; the electron density was controlled by applying a positive DC voltage to the gate in relation to the contacts. Saturating infrared illumination was applied to the samples for several minutes. This improved the quality of contacts and resulted in increased electron mobility [39,40]. The resistance of the contacts remained below 10 k Ω .

In addition to the double-gate samples, triple-gate samples were also used. The third gate was added to deplete the shunting channel between the contacts outside the Hall bar. This shunting channel can become prominent at the lowest electron densities in the insulating regime. The triple gate samples had Hall bar shapes with a width of 50 μm and a distance between the potential probes of 100 μm . The main NiCr/Al Hall-bar gate was fabricated similarly to that in the double-gate samples, with the difference that an approximately 200 nm thick SiO layer was evaporated. The contact gate was made by covering the structure with a ≈ 150 nm thick SiO layer and depositing a ≈ 40 nm thick aluminum gate on top of the SiO. An extra aluminum gate to deplete the shunting channel was fabricated simultaneously with the contact gate. For more details, see Ref. [38].

3. Results and Discussions

3.1. Double-threshold voltage-current curves as a signature of quantum electron solid; results obtained in Si MOSFETs

Figure 1 illustrates a series of low-temperature voltage-current curves measured at different electron densities within the insulating regime, where $n_s < n_c$. The critical density for the metal-insulator transition in this electron system is approximately $n_c \approx 8 \times 10^{10} \text{ cm}^{-2}$. The interaction parameter, which is defined as the ratio of the Coulomb energy to the Fermi energy, is given by $r_s = g_v / (\pi n_s)^{1/2} a_B$, where $g_v = 2$ denotes the valley degeneracy, n_s is the areal density of electrons, and a_B is the effective Bohr radius in the semiconductor. At these densities, the value r_s exceeds $r_s \sim 20$. For electron densities below approximately $6 \times 10^{10} \text{ cm}^{-2}$, two threshold voltages are observed. As the applied voltage increases, the current remains near zero until the voltage reaches a first threshold, V_{th1} . Once V_{th1} is surpassed, the current rises sharply until a second threshold voltage, V_{th2} , is reached. Beyond V_{th2} , the slope of the voltage-current curve decreases significantly, and the behavior becomes linear, although it is not ohmic (see also the top inset of Fig. 1). As the electron density is increased, the value of V_{th1} decreases, while the second threshold becomes less pronounced and eventually disappears. Notably, no hysteresis was observed within the range of electron densities studied.

Figure 2(a) displays the $V - I$ characteristics for the electron density of $n_s = 5.36 \times 10^{10} \text{ cm}^{-2}$ at various temperatures. As the temperature T increases, the second threshold voltage, V_{th2} , becomes less distinct, and the threshold behavior of the $V - I$

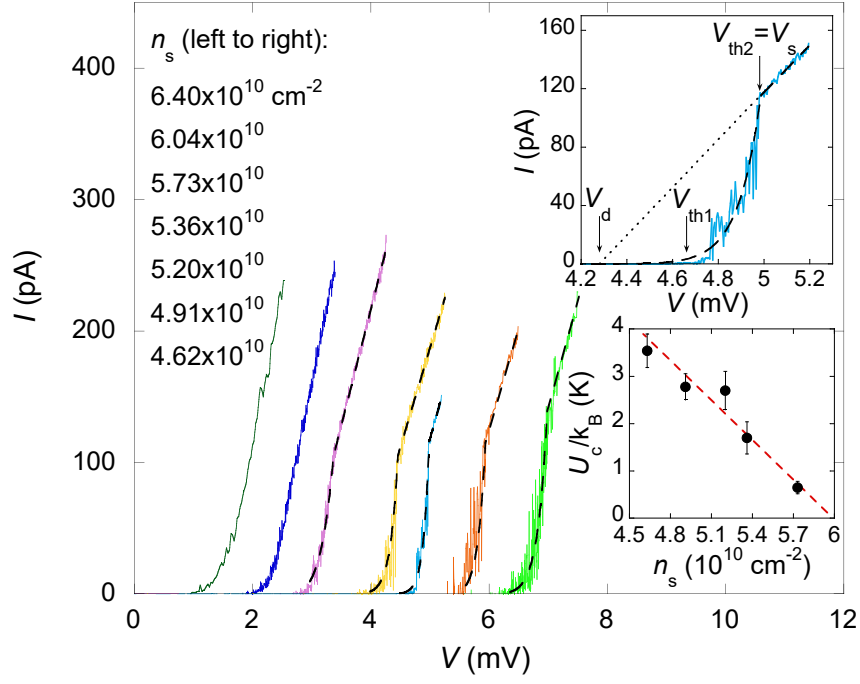


Figure 1. $V-I$ characteristics measured at different electron densities in the insulating state at a temperature of 60 mK. The dashed lines are fits to the data using Eq. (5). In the top inset, the $V-I$ curve for $n_s = 5.20 \times 10^{10} \text{ cm}^{-2}$ is shown on an expanded scale; the threshold voltages V_{th1} and V_{th2} , the static threshold $V_s = V_{th2}$, and the dynamic threshold V_d (which is obtained by extrapolating the linear portion of the curves to $I = 0$) are indicated. In the bottom inset, the activation energy U_c vs. electron density is plotted. The dashed line is a linear fit. Adapted from Ref. [32].

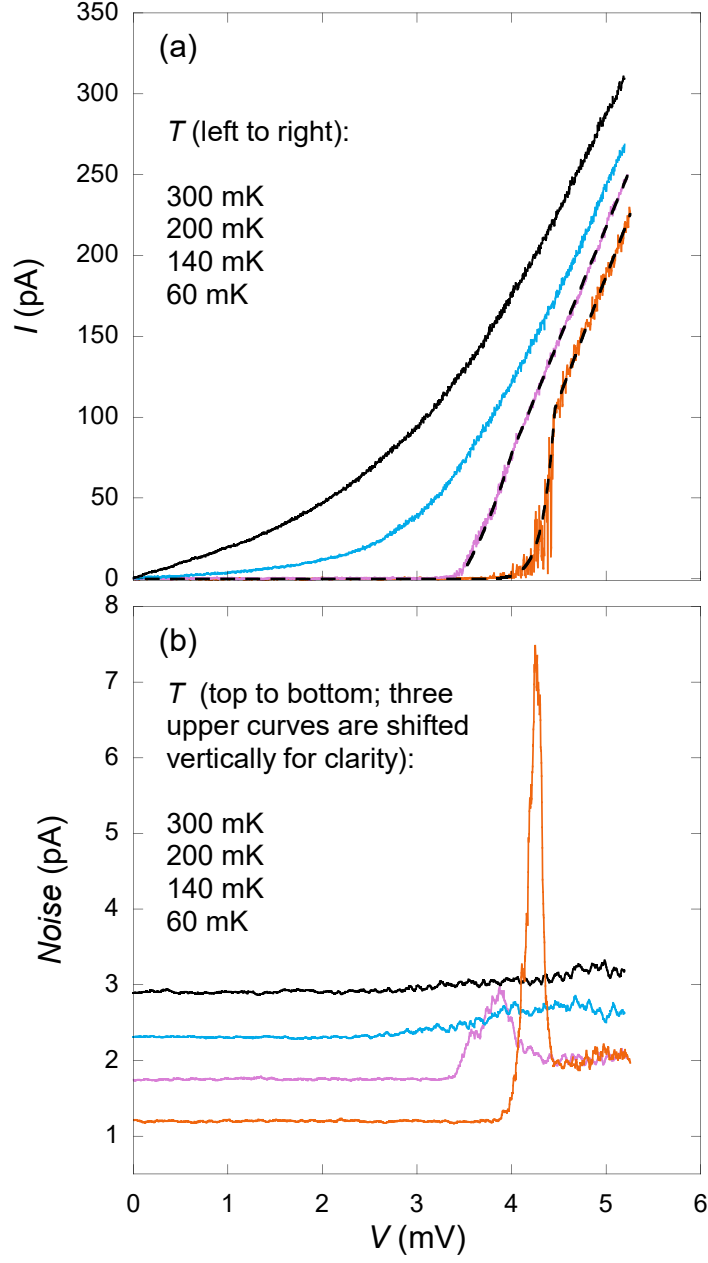


Figure 2. (a) $V - I$ characteristics measured at $n_s = 5.36 \times 10^{10} \text{ cm}^{-2}$ and different temperatures. The dashed lines are fits to the data using Eq. (5). (b) The broadband noise as a function of voltage for the same electron density and temperatures. Adapted from Ref. [32].

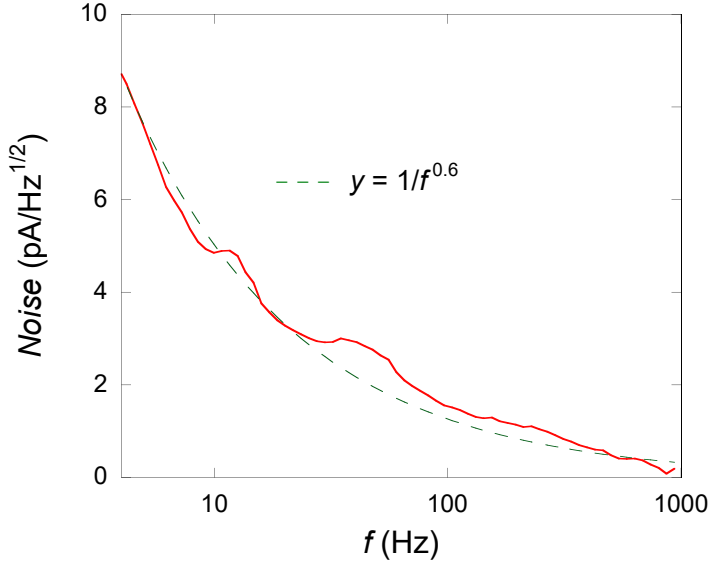


Figure 3. Noise as a function of frequency at $n_s = 5.36 \times 10^{10} \text{ cm}^{-2}$, $T = 60 \text{ mK}$, and $V = 4.26 \text{ mV}$ with resolution/bandwidth 2.5 Hz . The broad maxima at $f \sim 10$ and 60 Hz on the order of $1 \text{ pA}/\sqrt{\text{Hz}}$ are within the experimental uncertainty. The dashed line shows the $1/f^{0.6}$ dependence. Adapted from Ref. [32].

curves blurs.

The measured broadband noise is presented as a function of voltage in Fig. 2(b) for various temperatures, with an electron density of $n_s = 5.36 \times 10^{10} \text{ cm}^{-2}$. A significant increase in noise is observed between the thresholds V_{th1} and V_{th2} at the lowest temperature. This substantial noise decreases rapidly as the temperature increases, which is consistent with the two-threshold behavior seen in the $V - I$ curves shown in Fig. 2(a).

The spectrum of the generated noise, measured at its maximum value, is shown in Fig. 3. The noise level increases as the frequency, f , decreases, following the $1/f^\alpha$ law with $\alpha \approx 0.6$, which is close to one. This observation aligns with previous findings that indicated noise of the form $1/f^\alpha$ with α near one in the linear response regime of similar samples close to the metal-insulator transition [41,42].

There is a striking similarity between the double-threshold $V - I$ dependences in the insulating state of Si MOSFETs and those (with the voltage and current axes interchanged) known for the depinning of the vortex lattice in type-II superconductors (see, for example, Refs. [43–45]). The physics of the vortex lattice in type-II superconductors, in which the existence of two thresholds is well known, can be adapted for the case of an electron solid. The transient region between the dynamic (V_d) and static (V_s) thresholds corresponds to the collective pinning of the solid. In this region, the pinning occurs at the centers with different energies, and the current is thermally activated:

$$I \propto \exp \left[-\frac{U(V)}{k_B T} \right], \quad (1)$$

where $U(V)$ is the activation energy. The static threshold V_s signals the onset of the regime of solid motion with friction. This corresponds to the condition

$$eEL = U_c, \quad (2)$$

where E is the electric field and L is the characteristic distance between the pinning centers with maximal activation energy U_c . From the balance of the electric, pinning, and friction forces in the regime of solid motion with friction, one expects a linear $V - I$ characteristic that is offset by the threshold V_d corresponding to the pinning force

$$I = \sigma_0(V - V_d), \quad (3)$$

where σ_0 is a coefficient. Assuming that the activation energy for the Wigner solid is equal to

$$U(V) = U_c - eEL = U_c(1 - V/V_s), \quad (4)$$

the expression for the current is obtained:

$$I = \begin{cases} \sigma_0(V - V_d) & \text{if } V > V_s \\ \sigma_0(V - V_d) \exp \left[-\frac{U_c(1-V/V_s)}{k_B T} \right] & \text{if } V \leq V_s. \end{cases} \quad (5)$$

The fits to the data using Eq. (5) are shown by dashed lines in Figs. 1 and 2(a). As the figures show, the experimental two-threshold $V - I$ characteristics are described well by Eq. (5). The value of U_c decreases approximately linearly with electron density and tends to zero at $n_s \approx 6 \times 10^{10} \text{ cm}^{-2}$ (the bottom inset of Fig. 1). This is in contrast to the vanishing activation energy of electron-hole pairs at n_c obtained by measurements of the resistance in the limit of zero voltages/currents [46]. Presumably, the vanishing U_c is related to the minimum number of the strong pinning centers for which the collective pinning is still possible. The fact that the coefficient σ_0 is approximately constant ($\sigma_0 \approx 1.6 \times 10^{-7} \text{ Ohm}^{-1}$) indicates that weak pinning centers control the solid motion with friction [44]. Thus, the physics of the vortex lattice, adapted for the case of an electron solid, is relevant for the insulating state in a 2D electron system in silicon.

3.2. Generality of the double-threshold voltage-current curves for different classes of electron systems; results obtained in SiGe/Si/SiGe heterostructures

As inferred from both the level and character of the disorder potential, Si MOS-FETs and unprecedentedly high-mobility heterostructures, including SiGe/Si/SiGe heterostructures, belong to different classes of electron systems.

In Fig. 4(a), the V - I characteristics measured in the insulating regime at low electron densities ($r_s > 20$) in double-gate samples are presented. With increasing applied voltage, the current remains near zero up to a certain threshold voltage; beyond this

threshold, the current sharply increases, the threshold voltage increasing as the electron density decreases. However, these single-threshold V - I characteristics stop changing below $n_s \approx 6 \times 10^9 \text{ cm}^{-2}$. This indicates the presence of a shunting conduction channel outside the Hall bar that is obviously related to residual unintentional donor impurities in the SiGe/Si/SiGe heterostructures.

Applying a negative voltage to the additional gate in triple-gate samples depletes the shunting channel. However, the total depletion has not been reached, staying in the parallel-plate capacitor regime, in which the additional gate does not influence the transport properties of the 2D electron system in the main part of the sample. By suppressing the shunting channel, a significantly different behavior in the voltage-current characteristics is observed as the electron density decreases, as illustrated in Fig. 4(b). The $V - I$ characteristics show variations across the entire range of electron densities studied when the electron density is decreased. At the lowest electron densities, a second threshold voltage appears in the $V - I$ curves. These characteristics resemble those previously observed in Si MOSFETs [32]. This shows that the strongly interacting limit at low electron densities can be realized in the 2D electron system in SiGe/Si/SiGe heterostructures.

In Fig. 5(a), the typical voltage-current characteristics (upper panel) and the generated noise (lower panel) measured at a temperature of approximately 30 mK are presented. These measurements were conducted across different electron densities within the insulating regime (see also Fig. 5(b, c) for a more detailed view) [47]. These densities are below, but not too close to, the critical density $n_c \approx 8.8 \times 10^9 \text{ cm}^{-2}$, which signifies the transition from a metallic to an insulating state in the samples studied. At these specific values of n_s , the interaction parameter r_s exceeds 20. Notably, between the two threshold voltages, a peak in broadband current noise is observed, as shown in the lower panel of Fig. 5(a).

Figure 6(a) shows how the voltage-current characteristics and noise levels change with temperature. As the temperature rises, the voltage-current characteristics become less steep between the two threshold voltages, and the curves shift to lower voltages until the behavior associated with these two thresholds disappears. Similarly, the noise peak diminishes and eventually disappears as temperature increases. The inset of the upper panel in Fig. 6(a) features an Arrhenius plot of $I(T)$, which illustrates the activation temperature dependence down to approximately 60 mK. However, the data point collected at the lowest temperature deviates from this expected activation behavior, despite the electron temperature reached approximately 30 mK, as inferred from the analysis of Shubnikov-de Haas oscillations in the metallic regime. This deviation can be attributed to residual sample inhomogeneities, although the possible overheating effects in this experiment cannot be completely discounted.

In Fig. 7, the noise spectra at the maximum of noise measured at three different electron densities and a temperature of approximately 30 mK are presented. At high frequencies, the noise shows a more pronounced dependence on frequency as the electron density decreases, approaching a $1/f^\alpha$ dependence with $\alpha \approx 1$ for the two lowest densities. As the frequency decreases, the behavior at these two lowest densities changes to $1/f^\alpha$ with $\alpha \approx 0.2$, which is similar to the dependence observed at the highest electron density. This change in α occurs at a frequency that decreases with decreasing electron density.

Similarly to silicon MOSFETs, the observed results can be explained through a phenomenological theory of the collective depinning of elastic structures. This naturally produces a peak in broadband current noise between the dynamic and static thresholds, transitioning to the sliding of the solid over a pinning barrier once the static

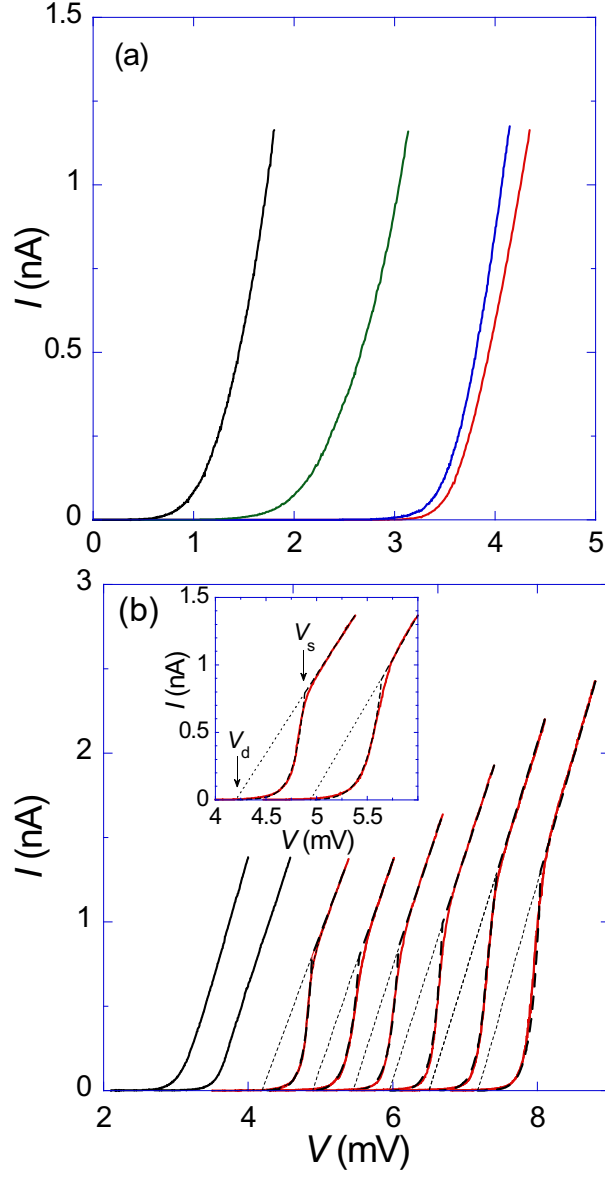


Figure 4. (a) The V - I characteristics measured in double-gate samples at various electron densities, displayed from left to right as follows: 7.95 , 6.98 , 6.21 , and $5.82 \times 10^9 \text{ cm}^{-2}$. The temperature is $T = 30$ mK. In panel (b), the V - I characteristics for triple-gate samples are shown at different electron densities, listed from left to right as: 6.37 , 6.19 , 6.01 , 5.92 , 5.83 , 5.74 , 5.65 , and $5.56 \times 10^9 \text{ cm}^{-2}$, also at $T = 30$ mK. The dashed lines represent fits to the data using Equation (5). The inset displays the V - I characteristics for electron densities of $n_s = 6.01 \times 10^9 \text{ cm}^{-2}$ and $5.92 \times 10^9 \text{ cm}^{-2}$ on an expanded scale. Arrows indicate the dynamic threshold voltage V_d , which is obtained by extrapolating (as shown by the dotted line) the linear portion of the V - I curves to zero current, along with the static threshold voltage V_s . From Ref. [38].

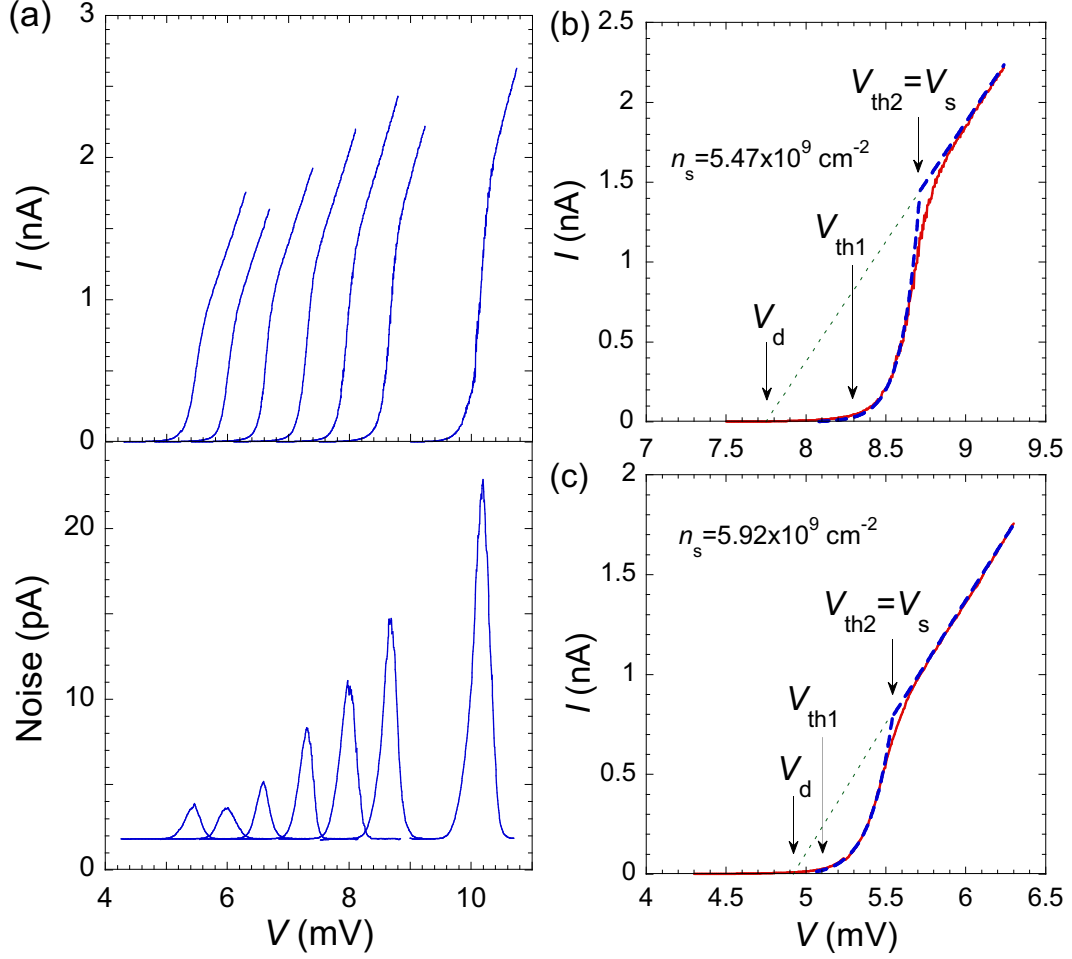


Figure 5. (a) The V - I characteristics are shown in the upper panel and the broadband noise is shown in the lower panel at a temperature of approximately 30 mK and various electron densities (from left to right): 5.92 , 5.83 , 5.74 , 5.65 , 5.56 , 5.47 , and $5.29 \times 10^9 \text{ cm}^{-2}$. Panels (b) and (c) display the V - I characteristics for two electron densities on an expanded scale. Also indicated are the threshold voltages, V_{th1} and V_{th2} , the dynamic threshold V_d , which is obtained by extrapolating the linear portion of the V - I curves to zero current, and the static threshold $V_s = V_{th2}$. The dashed lines are fits to the data using Eq. (5). From Ref. [47].

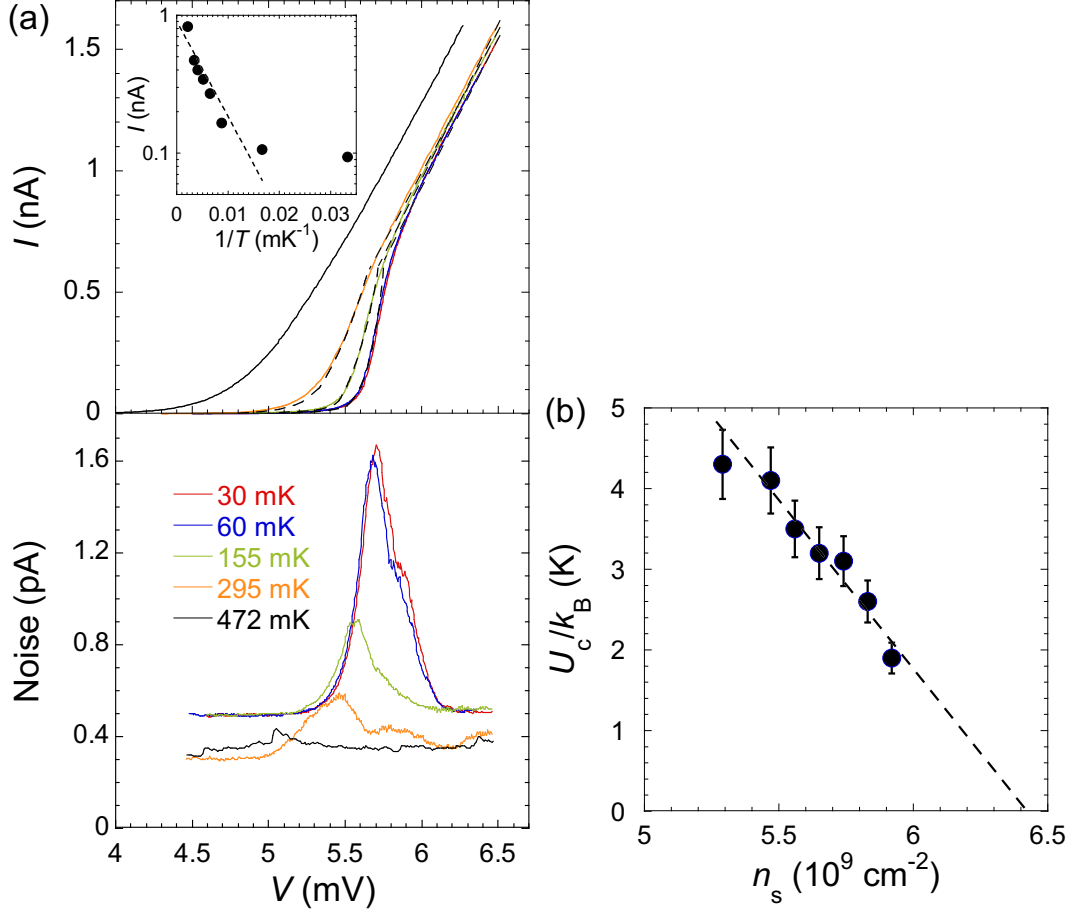


Figure 6. (a) The current (upper panel) and broadband noise (lower panel) are shown as a function of voltage at an electron density of $n_s = 5.83 \times 10^9$ cm $^{-2}$ for different temperatures in another sample. The curves in the upper panel are color-coded to correspond with the same temperatures presented in the lower panel. The overall noise is measured over the same frequency range as depicted in Fig. 7. The dashed lines represent fits to the data using Eq. (5). The inset includes an Arrhenius plot of $I(T)$ at $n_s = 5.83 \times 10^9$ cm $^{-2}$ and $V = 5.6$ mV. The dashed line is a linear fit that excludes the data point at 30 mK. (b) The activation energy U_c is plotted as a function of the electron density in the sample from Fig. 5. The dashed line indicates a linear fit. From Ref. [47].

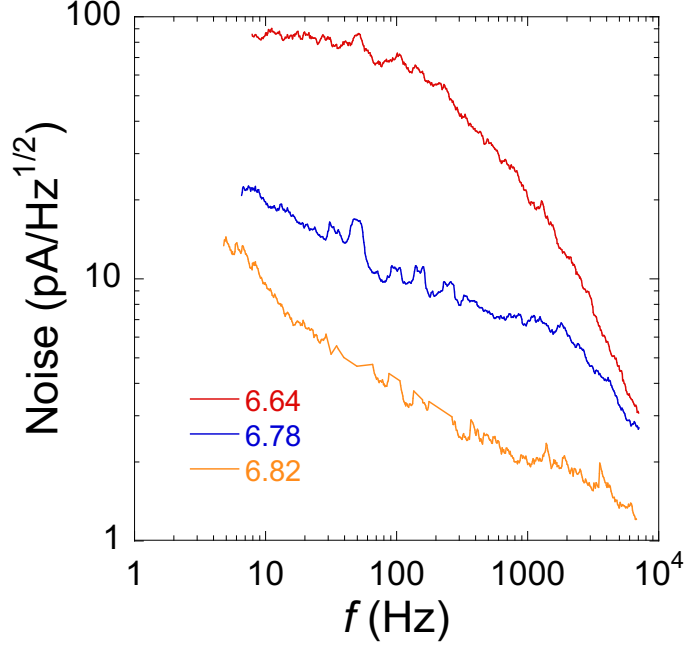


Figure 7. The frequency dependence of noise at the maximum at three electron densities indicated in units of 10^9 cm^{-2} and at $T \approx 30 \text{ mK}$ in another sample. From Ref. [47].

threshold is exceeded. The findings provide evidence for the formation of a quantum electron solid within this electron system and demonstrate the generality of this effect across different classes of electron systems.

3.3. Stabilization of the quantum electron solid in perpendicular magnetic fields in *SiGe/Si/SiGe* heterostructures

In Fig. 8(a), a set of voltage-current characteristics is displayed. The curves are measured at a temperature of 60 mK in zero magnetic field at different electron densities in the insulating regime $n_s < n_c$ (here $n_c \approx 0.7 \times 10^{10} \text{ cm}^{-2}$ is the critical density for the metal-insulator transition in the samples used); the corresponding interaction parameter r_s exceeds 20 at these values of n_s . Two-threshold voltage-current curves are observed at electron densities below $n_s \approx 0.3 \times 10^{10} \text{ cm}^{-2}$ [48].

In Fig. 8(b), $V - I$ curves at a temperature of $T = 60 \text{ mK}$ for $B = 3 \text{ T}$ are shown. The figure shows that the double-threshold behavior occurs at voltages that are an order of magnitude lower and at significantly higher electron densities compared to the case without a magnetic field. A peak in broadband current noise is observed between the two threshold voltages, whether or not a magnetic field is present (not shown here).

Voltage-current characteristics at a temperature of $T = 60 \text{ mK}$ for $n_s = 1.67 \times 10^{10} \text{ cm}^{-2}$ under various magnetic fields are illustrated in Fig. 8(c). As the magnetic field is increased, the double-threshold voltage-current curves emerge.

In Fig. 9(a), the voltage V_{onset} is shown, which is determined by linearly extrapolating the $V - I$ curve at the onset of the double-threshold behavior at $T = 30 \text{ mK}$ to zero current. This voltage is plotted as a function of the magnetic field. V_{onset} decreases by an order of magnitude as the magnetic field increases up to $B \approx 2 \text{ T}$. Beyond this point, in higher magnetic fields, the value of V_{onset} continues to decrease with

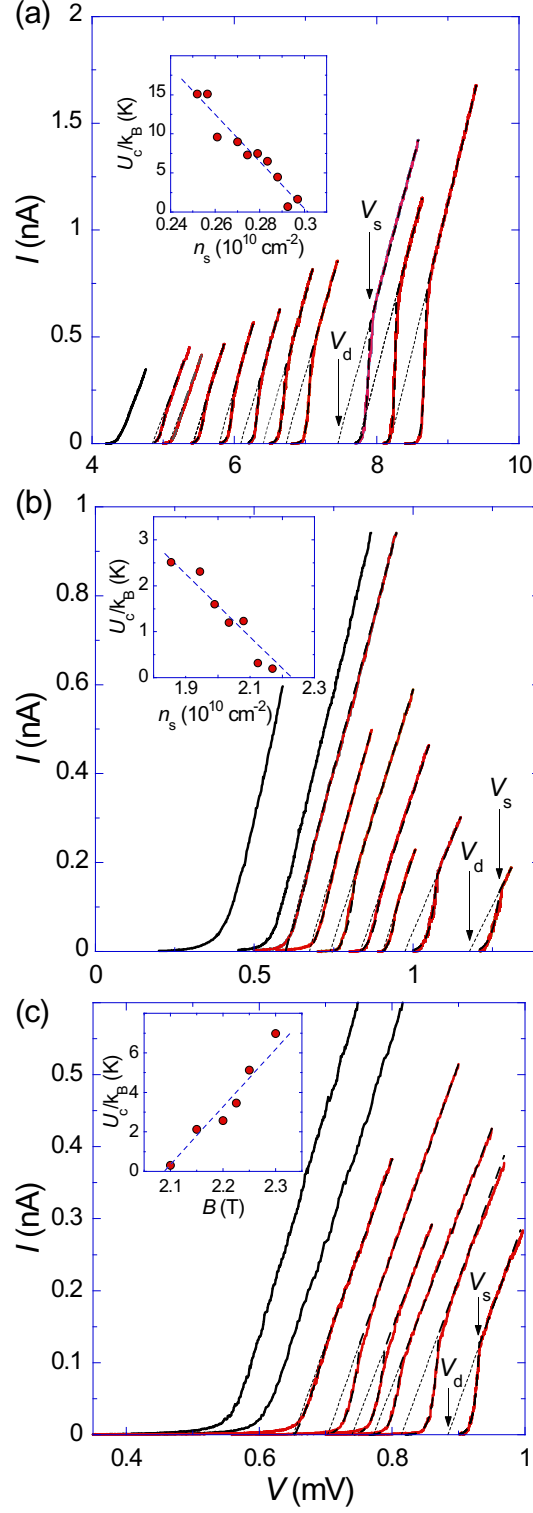


Figure 8. (a) Voltage-current characteristics in zero magnetic field at $T = 60$ mK at electron densities (in units of 10^{10} cm^{-2} , left to right): 0.306, 0.297, 0.293, 0.288, 0.284, 0.279, 0.275, 0.270, 0.261, 0.257, 0.252. (b) Voltage-current characteristics in $B = 3$ T at $T = 60$ mK at electron densities (in units of 10^{10} cm^{-2} , left to right): 2.30, 2.21, 2.17, 2.12, 2.08, 2.03, 1.99, 1.94, 1.85. (c) Voltage-current characteristics at $T = 60$ mK for $n_s = 1.67 \times 10^{10} \text{ cm}^{-2}$ in different magnetic fields (left to right): 2, 2.05, 2.1, 2.15, 2.2, 2.225, 2.25, and 2.3 T. Also shown are the dynamic threshold V_d obtained by the extrapolation (dotted line) of the linear part of the V - I curves to zero current and the static threshold V_s . The dashed lines are fits to the data using Eq. (5). Insets: activation energy U_c as a function of the electron density in (a, b) and the magnetic field in (c). The dashed line is a linear fit. From Ref. [48].

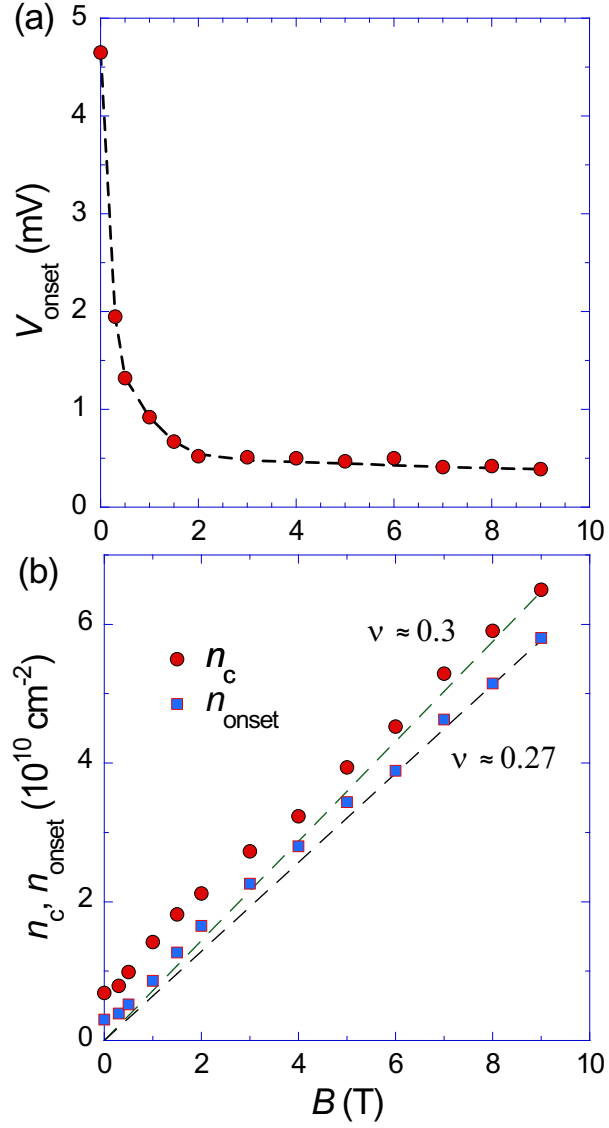


Figure 9. (a) The voltage V_{onset} for the onset of the double-threshold V - I curves at $T = 30$ mK as a function of the magnetic field. The dashed line is a guide to the eye. (b) The corresponding electron density n_{onset} for the onset of the double-threshold V - I curves at $T = 30$ mK as a function of the magnetic field (squares). Also shown is the critical density n_c for the metal-insulator transition versus magnetic field (circles). The dashed lines indicate the slopes of the dependences at high B . From Ref. [48].

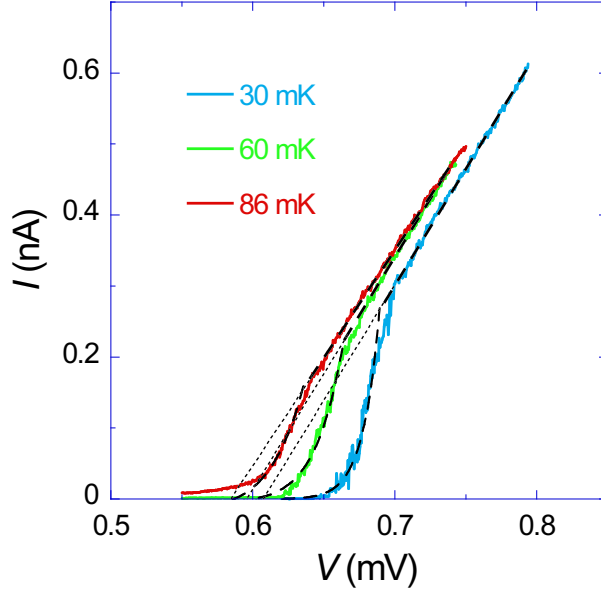


Figure 10. Voltage-current characteristics at $B = 4$ T and $n_s = 2.72 \times 10^{10} \text{ cm}^{-2}$ at different temperatures. The fits corresponding to the activation energy $U_c = 1.5$ K in Eq. (5) are shown by dashed lines. From Ref. [48].

increasing B , although at a much slower rate.

In Figure 9(b), the electron density n_{onset} at the onset of the double-threshold voltage-current curves measured at $T = 30$ mK is plotted as a function of the magnetic field (represented by squares). Also included is the critical density n_c for the metal-insulator transition versus the magnetic field (represented by circles). This critical density is determined by the vanishing nonlinearity of the $V - I$ curves when extrapolated from the insulating phase, as detailed in Ref. [49]. Both n_{onset} and n_c increase with the magnetic field. Notably, for all magnetic fields considered, n_{onset} remains below n_c . At high magnetic fields, both quantities tend to linear dependences that correspond to a filling factor of $\nu = n_s \hbar c / e B \approx 0.27$ for n_{onset} and $\nu \approx 0.3$ for n_c .

In Fig. 10, the V - I characteristics at a magnetic field of $B = 4$ T and electron density of $n_s = 2.72 \times 10^{10} \text{ cm}^{-2}$ are presented at different temperatures. The fits corresponding to the activation energy $U_c = 1.5$ K accurately describe the data. Unlike the case at $B = 0$, where the V - I curves saturate below $T = 60$ mK [47], the V - I curves in a strong magnetic field exhibit the expected temperature dependence down to $T = 30$ mK. This indicates no overheating down to the lowest temperatures used in the experiments.

The observed increase in the onset density n_{onset} for the double-threshold V - I curves in response to increasing magnetic field indicates that the quantum electron solid is becoming more stabilized in perpendicular magnetic fields. This finding aligns with theoretical predictions that applying a perpendicular magnetic field should encourage the formation of a Wigner solid by reducing the amplitude of zero-point vibrations of the electrons at their lattice sites [50–53]. The corresponding filling factor $\nu \approx 0.27$ observed in this two-valley 2D electron system is reasonably consistent with theoretical expectations, which indicate that in a disorderless single-valley 2D electron system, the Wigner crystal should form at filling factors $\nu \lesssim 0.15$ [54,55]. The intermediate insulating region between $n_{\text{onset}}(B)$ and $n_c(B)$, which precedes the formation of the

electron solid, may be attributed to a fluctuation region. Additionally, the observed decrease in the onset voltage V_{onset} for the double-threshold V - I curves with increasing magnetic field also reflects the stabilizing effects of the magnetic field. Qualitatively, the behavior of V_{onset} can be explained as follows: in a zero magnetic field, the amplitude of the zero-point vibrations of the electrons at their lattice sites is relatively large, allowing for easy deformation of the electron solid near the pinning centers. Consequently, electrons should be strongly pinned by these centers, leading to a relatively high onset voltage. Conversely, in strong perpendicular magnetic fields, this relationship reverses. The increased rigidity or uniformity of the electron solid in the magnetic fields may also account for the pronounced temperature dependence of the V - I curves observed down to the lowest temperatures, which is not seen at $B = 0$.

3.4. Inequivalence of the low-density insulating state and quantum Hall insulating states in SiGe/Si/SiGe heterostructures

There have been claims of the detection of the Wigner crystal at low Landau fillings in the 2D carrier system in AlGaAs/GaAs heterojunctions, based on the observation of resonance in the real part of frequency-dependent diagonal microwave conductivity that was interpreted as the pinning mode of Wigner crystal domains oscillating in the disorder potential (see, *e.g.*, Refs. [14,56–60]). Similar resonances were observed in AlGaAs/GaAs 2D electron systems in the quantum Hall regime near integer and fractional Landau fillings and interpreted as originating from a Wigner crystal state formed by quasi-particles with density determined by the deviation from the integer or fractional filling factor [61–67].

The voltage-current (V - I) characteristics measured at different electron densities in the low-density insulating state at a magnetic field of $B = 4$ T and a temperature of $T = 30$ mK are shown in Fig. 11(a) [68]; here, the voltage is applied between the Hall potential probes for the configuration to be relevant for comparison with the data measured near Landau filling factors $\nu = 1$ and $\nu = 2$. At electron densities below $n_s \approx 0.26 \times 10^{11} \text{ cm}^{-2}$, two-threshold voltage-current curves are observed. As the electron density decreases and one moves further into the low-density insulating state, the double-threshold V - I curves shift to higher voltages. This behavior is similar to what has been observed in Refs. [32,47,48,69] and discussed in earlier sections.

In Figs. 11(b,c), the $V - I$ curves are shown, which are recalculated from breakdown dependences of the longitudinal voltage V_{xx} on source-drain current I_{sd} at different electron densities in a fixed magnetic field at $T = 30$ mK for the quantum Hall insulating states near Landau filling factors $\nu = 1$ and $\nu = 2$. As long as the magnetoresistivity ρ_{xx} is much smaller than the Hall resistivity $\rho_{xy} = h/\nu_0 e^2$ (here ν_0 is an integer), the dissipative current I between the opposite edges of the sample and the Hall voltage V are related to the measured values through the quantized value of ρ_{xy} : $I = V_{xx}/\rho_{xy}$ and $V = I_{sd}\rho_{xy}$, where the measured value V_{xx} should be normalized by the aspect ratio. The dependence $I(V)$ is a voltage-current characteristic equivalent to the Corbino geometry case [30]. These characteristics look similar near $\nu = 1$ and $\nu = 2$. At the maximum deviations $\Delta n_s = |\nu - \nu_0|eB/hc$, the current increases sharply with increasing applied voltage, and then the slope of the V - I curves decreases, corresponding to an approximately proportional increase of the current with voltage. As one enters the quantum Hall insulating state by reducing the deviation Δn_s , the initial steep rise of the current and the reduction in the slope of the V - I curves disappear. The obtained V - I curves are in contrast to the double-threshold V - I characteristics

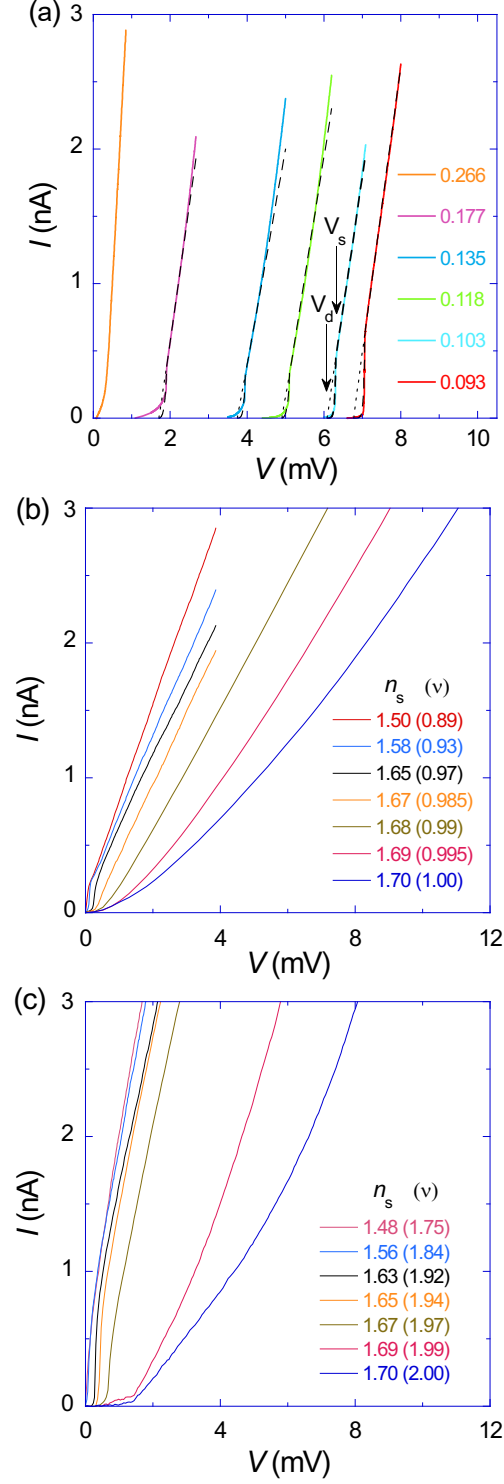


Figure 11. (a) Voltage-current characteristics at different electron densities in the low-density insulating state at $B = 4$ T and $T = 30$ mK. The electron densities are indicated in units of 10^{11} cm^{-2} . Also shown are the dynamic threshold V_d obtained by the extrapolation (dotted line) of the linear part of the V - I curves to zero current and the static threshold V_s . The dashed lines are fits to the data using Eq. (5). (b) Voltage-current characteristics recalculated from the I_{sd} - V_{xx} data at different electron densities at $T = 30$ mK in $B = 7$ T for $\nu \leq 1$. The electron densities are indicated in units of 10^{11} cm^{-2} , along with the filling factors in brackets. (c) Voltage-current characteristics recalculated from the I_{sd} - V_{xx} data at different electron densities at $T = 30$ mK in $B = 3.5$ T for $\nu \leq 2$. The electron densities are indicated in units of 10^{11} cm^{-2} , along with the filling factors in brackets. Adapted from Ref. [68].

in the low-density insulating state from Fig. 11(a). It should be emphasized that the qualitative difference between the V - I curves in the low-density insulating state and quantum Hall insulating states is observed in similar ranges of voltages, currents, and electron densities (n_s) or quasi-particle densities (Δn_s).

Assuming the existence of a Wigner crystal state formed by quasi-particles with density determined by the deviation from the integer filling factor, one expects similar data in the low-density insulating state and quantum Hall insulating states, according to Refs. [61–67]. It should be emphasized that the key idea underlying this assumption is that the quasi-particles can be considered separately as an independent subsystem. However, the experimental results obtained in the 2D electron system in SiGe/Si/SiGe quantum wells do not confirm the occurrence of a quasi-particle quantum Hall Wigner solid. The low-density insulating state is characterized by the observed double-threshold voltage-current curves, which serve as a signature of the quantum Wigner solid [32,47,48,69]. In contrast, significantly different V - I curves are observed in the integer quantum Hall insulating states. This finding indicates that the quasi-particles near integer filling do not form an independent subsystem. A possible reason may be the mixing of Landau levels due to electron-electron interactions that strongly exceed the cyclotron energy in this 2D electron system. For comparison, the 2D electron system in AlGaAs/GaAs heterostructures, where similar data were reported in the low-density insulating state and quantum Hall insulating states, is characterized by electron-electron interactions that are comparable to the cyclotron energy due to an appreciably smaller (by a factor of about 3) effective mass, in which case the mixing of Landau levels is expected to be less relevant. This difference can be essential in interpreting the experimental results in both electron systems.

4. Conclusions

Two-threshold voltage-current characteristics, accompanied by a peak in broadband current noise occurring between these two threshold voltages, have been observed in the insulating regime at low electron densities in 2D electron systems within Si MOSFETs and ultra-high mobility SiGe/Si/SiGe heterostructures. These findings can be explained by a phenomenological theory of the collective depinning of elastic structures, which naturally generates a peak in broadband current noise between the dynamic and static thresholds, transitioning to the sliding of the solid over a pinning barrier above the static threshold. The obtained results provide evidence for the formation of a quantum electron solid in these electron systems and demonstrate the generality of this effect across different classes of electron systems. Furthermore, applying a perpendicular magnetic field promotes the double-threshold behavior, allowing it to occur at voltages that are an order of magnitude lower and at significantly higher electron densities compared to the zero-field case. This indicates the stabilization of the quantum electron solid, aligning with theoretical predictions. The double-threshold voltage-current curves, representative of electron solid formation at low densities, are not observed in the quantum Hall regime, which does not confirm the existence of a quasi-particle quantum Hall Wigner solid and indicates that quasi-particles near integer filling do not form an independent subsystem.

Disclosure statement

The authors declare no conflict of interest.

Funding

This investigation was supported by the RF state task.

References

- [1] Wigner E. On the interaction of electrons in metals. *Phys Rev.* 1934;46:1002–1011.
- [2] Chaplik AV. Possible crystallization of charge carriers in low-density inversion layers. *Sov Phys JETP.* 1972;35:395–398.
- [3] Tanatar B, Ceperley DM. Ground state of the two-dimensional electron gas. *Phys Rev B.* 1989;39:5005–5016.
- [4] Shashkin AA, Kravchenko SV, Dolgoplov VT, et al. Indication of the ferromagnetic instability in a dilute two-dimensional electron system. *Phys Rev Lett.* 2001;87:086801.
- [5] Shashkin AA, Kravchenko SV, Dolgoplov VT, et al. Sharp increase of the effective mass near the critical density in a metallic two-dimensional electron system. *Phys Rev B.* 2002;66:073303.
- [6] Attacalite C, Moroni S, Gori-Giorgi P, et al. Correlation energy and spin polarization in the 2D electron gas. *Phys Rev Lett.* 2002;88:256601.
- [7] Spivak B, Kivelson SA. Phases intermediate between a two-dimensional electron liquid and Wigner crystal. *Phys Rev B.* 2004;70:155114.
- [8] Shashkin AA, Anissimova S, Sakr MR, et al. Pauli spin susceptibility of a strongly correlated two-dimensional electron liquid. *Phys Rev Lett.* 2006;96:036403.
- [9] Mokashi A, Li S, Wen B, et al. Critical behavior of a strongly interacting 2D electron system. *Phys Rev Lett.* 2012;109:096405.
- [10] Melnikov MY, Shashkin AA, Dolgoplov VT, et al. Indication of band flattening at the Fermi level in a strongly correlated electron system. *Sci Rep.* 2017;7:14539.
- [11] Kagalovsky V, Kravchenko SV, Nemirovsky D. Hartree-Fock description of a Wigner crystal in two dimensions. *Physica E.* 2020;119:114016.
- [12] Grimes CC, Adams G. Evidence for a liquid-to-crystal phase transition in a classical, two-dimensional sheet of electrons. *Phys Rev Lett.* 1979 Mar;42:795–798.
- [13] Andrei EY, Deville G, Glatli DC, et al. Observation of a magnetically induced Wigner solid. *Phys Rev Lett.* 1988;60:2765–2768.
- [14] Williams FIB, Wright PA, Clark RG, et al. Conduction threshold and pinning frequency of magnetically induced Wigner solid. *Phys Rev Lett.* 1991;66:3285–3288.
- [15] Goldman VJ, Santos M, Shayegan M, et al. Evidence for two-dimensional quantum Wigner crystal. *Phys Rev Lett.* 1990;65:2189–2192.
- [16] Jiang HW, Willett RL, Stormer HL, et al. Quantum liquid versus electron solid around $\nu=1/5$ Landau-level filling. *Phys Rev Lett.* 1990 Jul;65:633–636.
- [17] Jiang HW, Stormer HL, Tsui DC, et al. Magnetotransport studies of the insulating phase around $\nu = 1/5$ Landau-level filling. *Phys Rev B.* 1991;44:8107–8114.
- [18] D'Iorio M, Pudalov VM, Semenchinsky SG. Reentrant insulating phase in Si inversion layers in low magnetic fields. *Phys Rev B.* 1992;46:15992–16004.
- [19] Pudalov VM, D'Iorio M, Kravchenko SV, et al. Zero-magnetic-field collective insulator phase in a dilute 2D electron system. *Phys Rev Lett.* 1993;70:1866–1869.
- [20] Giamarchi T. Electronic glasses. In: *Quantum phenomena in mesoscopic systems.* IOS Press; 2003. p. 303–339.

- [21] Qiu RLJ, Gao XPA, Pfeiffer LN, et al. Connecting the reentrant insulating phase and the zero-field metal-insulator transition in a 2D hole system. *Phys Rev Lett.* 2012;108:106404.
- [22] Knighton T, Wu Z, Tarquini V, et al. Reentrant insulating phases in the integer quantum Hall regime. *Phys Rev B.* 2014 Oct;90:165117.
- [23] Qiu R, Liu CW, Liu S, et al. New reentrant insulating phases in strongly interacting 2D systems with low disorder. *Appl Sci.* 2018;8:1909.
- [24] Knighton T, Wu Z, Huang J, et al. Evidence of two-stage melting of Wigner solids. *Phys Rev B.* 2018;97:085135.
- [25] Falson J, Sodemann I, Skinner B, et al. Competing correlated states around the zero-field Wigner crystallization transition of electrons in two dimensions. *Nat Mater.* 2022 Mar; 21(3):311–316.
- [26] Hossain MS, Ma MK, Villegas-Rosales KA, et al. Anisotropic two-dimensional disordered Wigner solid. *Phys Rev Lett.* 2022 Jul;129:036601.
- [27] Madathil PT, Rosales KAV, Chung YJ, et al. Moving crystal phases of a quantum Wigner solid in an ultra-high-quality 2D electron system. *Phys Rev Lett.* 2023 Dec;131:236501.
- [28] Marianer S, Shklovskii BI. Effective temperature of hopping electrons in a strong electric field. *Phys Rev B.* 1992;46:13100–13103.
- [29] Dolgoplov VT, Kravchenko GV, Shashkin AA, et al. Metal-insulator transition in Si inversion layers in the extreme quantum limit. *Phys Rev B.* 1992;46:13303–13308.
- [30] Shashkin AA, Dolgoplov VT, Kravchenko GV. Insulating phases in a two-dimensional electron system of high-mobility Si MOSFET's. *Phys Rev B.* 1994 May;49:14486–14495.
- [31] Shashkin AA. Metal-insulator transitions and the effects of electron-electron interactions in two-dimensional electron systems. *Phys Usp.* 2005 feb;48:129–149.
- [32] Brussarski P, Li S, Kravchenko SV, et al. Transport evidence for a sliding two-dimensional quantum electron solid. *Nat Commun.* 2018;9:3803.
- [33] Heemskerk R, Klapwijk TM. Nonlinear resistivity at the metal-insulator transition in a two-dimensional electron gas. *Phys Rev B.* 1998 Jul;58:R1754–R1757.
- [34] Lu TM, Tsui DC, Lee CH, et al. Observation of two-dimensional electron gas in a Si quantum well with mobility of $1.6 \times 10^6 \text{ cm}^2/\text{Vs}$. *Appl Phys Lett.* 2009;94:182102.
- [35] Lu TM, Tsui DC, Lee CH, et al. Erratum: “Observation of two-dimensional electron gas in a Si quantum well with mobility of $1.6 \times 10^6 \text{ cm}^2/\text{Vs}$ ”. *Appl Phys Lett.* 2010;97:059904.
- [36] Huang SH, Lu TM, Lu SC, et al. Mobility enhancement of strained Si by optimized SiGe/Si/SiGe structures. *Appl Phys Lett.* 2012;101(4):42111.
- [37] Schäffler F. High-mobility Si and Ge structures. *Semicond Sci Technol.* 1997 dec; 12(12):1515.
- [38] Melnikov MY, Shashkin AA, Huang SH, et al. Triple-top-gate technique for studying the strongly interacting 2D electron systems in heterostructures. *Appl Phys Lett.* 2024 10; 125(15):153102.
- [39] Melnikov MY, Shashkin AA, Dolgoplov VT, et al. Ultra-high mobility two-dimensional electron gas in a SiGe/Si/SiGe quantum well. *Appl Phys Lett.* 2015;106:092102.
- [40] Melnikov MY, Dolgoplov VT, Shashkin AA, et al. Unusual anisotropy of inplane field magnetoresistance in ultra-high mobility SiGe/Si/SiGe quantum wells. *J Appl Phys.* 2017; 122:224301.
- [41] Jaroszyński J, Popović D, Klapwijk TM. Universal behavior of the resistance noise across the metal-insulator transition in silicon inversion layers. *Phys Rev Lett.* 2002 Dec; 89:276401.
- [42] Jaroszyński J, Popović D, Klapwijk TM. Magnetic-field dependence of the anomalous noise behavior in a two-dimensional electron system in silicon. *Phys Rev Lett.* 2004 Jun; 92:226403.
- [43] Yeh WJ, Kao YH. Flux-flow noise in type-II superconductors. *Phys Rev B.* 1991 Jul; 44:360–373.
- [44] Blatter G, Feigel'man MY, Geshkenbein YB, et al. Vortices in high-temperature superconductors. *Rev Mod Phys.* 1994;66:1125–1388.
- [45] Bullard TJ, Das J, Daquila GL, et al. Vortex washboard voltage noise in type-II super-

- conductors. *Eur Phys J B*. 2008 Oct;65(4):469.
- [46] Shashkin AA, Kravchenko SV, Klapwijk TM. Metal-insulator transition in a 2D electron gas: Equivalence of two approaches for determining the critical point. *Phys Rev Lett*. 2001;87:266402.
 - [47] Melnikov MY, Shashkin AA, Huang SH, et al. Collective depinning and sliding of a quantum Wigner solid in a two-dimensional electron system. *Phys Rev B*. 2024 Jan; 109:L041114.
 - [48] Melnikov MY, Smirnov DG, Shashkin AA, et al. Stabilization of a two-dimensional quantum electron solid in perpendicular magnetic fields. *Phys Rev B*. 2025 Jan;111:L041301.
 - [49] Melnikov MY, Shashkin AA, Dolgoplov VT, et al. Quantum phase transition in ultrahigh mobility SiGe/Si/SiGe two-dimensional electron system. *Phys Rev B*. 2019;99:081106(R).
 - [50] Lozovik YE, Yudson VI. Crystallization of a two-dimensional electron gas in a magnetic field. *JETP Lett*. 1975;22:11–12.
 - [51] Ulinich FP, Usov NA. Phase diagram of a two-dimensional Wigner crystal in a magnetic field. *Sov Phys JETP*. 1979;49:147–150.
 - [52] Fukuyama H. Two-dimensional Wigner crystal under magnetic field. *Solid State Commun*. 1975;17(10):1323–1326.
 - [53] Eguiluz AG, Maradudin AA, Elliott RJ. Two-dimensional Wigner lattice in a magnetic field and in the presence of a random array of pinning centers. *Phys Rev B*. 1983 Apr; 27:4933–4945.
 - [54] Lam PK, Girvin SM. Liquid-solid transition and the fractional quantum-Hall effect. *Phys Rev B*. 1984 Jul;30:473–475.
 - [55] Levesque D, Weis JJ, MacDonald AH. Crystallization of the incompressible quantum-fluid state of a two-dimensional electron gas in a strong magnetic field. *Phys Rev B*. 1984 Jul;30:1056–1058.
 - [56] Engel LW, Li CC, Shahar D, et al. Microwave resonances in low-filling insulating phase of two-dimensional electron system. *Solid State Commun*. 1997;104(3):167–171.
 - [57] Ye PD, Engel LW, Tsui DC, et al. Correlation lengths of the Wigner-crystal order in a two-dimensional electron system at high magnetic fields. *Phys Rev Lett*. 2002 Oct; 89:176802.
 - [58] Sambandamurthy G, Wang Z, Lewis RM, et al. Pinning mode resonances of new phases of 2D electron systems in high magnetic fields. *Solid State Commun*. 2006;140(2):100–106. Emergent phenomena in quantum Hall systems.
 - [59] Moon BH, Engel LW, Tsui DC, et al. Pinning modes of high-magnetic-field Wigner solids with controlled alloy disorder. *Phys Rev B*. 2014 Feb;89:075310.
 - [60] Freeman ML, Madathil PT, Pfeiffer LN, et al. Origin of pinning disorder in magnetic-field-induced Wigner solids. *Phys Rev Lett*. 2024 Apr;132:176301.
 - [61] Chen Y, Lewis RM, Engel LW, et al. Microwave resonance of the 2D Wigner crystal around integer Landau fillings. *Phys Rev Lett*. 2003 Jul;91:016801.
 - [62] Lewis RM, Chen Y, Engel LW, et al. Evidence of a first-order phase transition between Wigner-crystal and bubble phases of 2D electrons in higher Landau levels. *Phys Rev Lett*. 2004 Oct;93:176808.
 - [63] Lewis RM, Chen Y, Engel LW, et al. Wigner crystallization about $\nu=3$. *Physica E: Low-dimensional Systems and Nanostructures*. 2004;22(1):104–107. 15th International Conference on Electronic Properties of Two-Dimensional Systems (EP2DS-15).
 - [64] Zhu H, Chen YP, Jiang P, et al. Observation of a pinning mode in a Wigner solid with $\nu = 1/3$ fractional quantum Hall excitations. *Phys Rev Lett*. 2010 Sep;105:126803.
 - [65] Hatke AT, Liu Y, Magill BA, et al. Microwave spectroscopic observation of distinct electron solid phases in wide quantum wells. *Nat Commun*. 2014 Jun;5(1):4154.
 - [66] Moon BH, Engel LW, Tsui DC, et al. Microwave pinning modes near Landau filling $\nu = 1$ in two-dimensional electron systems with alloy disorder. *Phys Rev B*. 2015 Jul;92:035121.
 - [67] Kim KS, Kivelson SA. The quantum Hall effect in the absence of disorder. *npj Quantum Materials*. 2021 Mar;6(1):22.
 - [68] Melnikov MY, Smirnov DG, Shashkin AA, et al. Inequivalence of the low-density insu-

lating state and quantum Hall insulating states in a strongly correlated two-dimensional electron system. Phys Rev B. 2025 Oct;112:165309.

- [69] Shashkin AA, Melnikov MY, Kravchenko SV. Transport evidence for the quantum Wigner solid formation in two-dimensional electron systems. Physica E: Low-dimensional Systems and Nanostructures. 2025;168:116192.